



Forced Ignition of a Rich Hydrogen/Air Mixture in a Laminar Counterflow: A Computational Study

Shumeng Xie¹ · Xinyi Chen¹ · Hannes Böttler² · Arne Scholtissek² · Christian Hasse² · Zheng Chen¹

Received: 13 April 2022 / Accepted: 26 September 2022 / Published online: 1 October 2022
© The Author(s), under exclusive licence to Springer Nature B.V. 2022

Abstract

Forced ignition has broad application in engines. Usually fuel-lean mixtures of large hydrocarbons are used in engines and they have large Lewis numbers, Le . Due to the high positive stretch of the expanding ignition kernel, it is very difficult to ignite a mixture with very large Le . In this study, the forced ignition of a fuel-rich H_2 /air mixture with $Le \approx 2.3$ in a laminar counterflow is investigated via two-dimensional simulations. The emphasis is placed on assessing the flow effects on ignition in mixtures with large Le . The transient ignition kernel development and the minimum ignition energy (MIE) at different strain rates and different ignition positions are studied. The counterflow is found to greatly affect the ignition kernel development and MIE for $Le \approx 2.3$. The counterflow compresses the ignition kernel and changes its shape from a sphere to an oblate spheroid. Consequently, the flame propagating in the axial direction is strengthened since its curvature is reduced and $Le > 1$; while the opposite occurs to the flame propagating in the radial direction. With the increase of strain rate, the radial flame has a negative displacement speed and extinguishes, and thereby the MIE increases. To achieve successful ignition at large Le and at high strain rate, a strong anchored axial flame needs to be formed. Counterintuitively, it is found that moving the ignition position away from the stagnation point can reduce the MIE and thereby promote ignition for the present mixture with large Le . Such ignition enhancement is caused by the reduction of the flame curvature of the flame propagating in the radial direction. The change of the density-weighted displacement speed with the Karlovitz number is also studied for the transient ignition process; and strong unsteadiness is observed. This work provides insights on better understanding of the ignition of mixtures with $Le > 2$ under strained conditions.

Keywords Forced ignition · Large Lewis number · Counterflow · Strain rate · Minimum ignition energy

✉ Zheng Chen
cz@pku.edu.cn

¹ SKLTCS, CAPT, BIC-ESAT, College of Engineering, Peking University, Beijing 100871, China

² Department of Mechanical Engineering, Simulation of reactive Thermo-Fluid Systems, Technical University of Darmstadt, Otto-Berndt-Str. 2, 64287 Darmstadt, Germany

1 Introduction

Flame ignition is a fundamental and ubiquitous problem in combustion. It occurs in most practical combustion devices, e.g., spark ignition engine (SIE) and gas turbine engine; and it is also closely related to fire safety (Lewis and von Elbe 1961; Mastorakos 2017). Understanding ignition is important for developing advanced combustion engines. For an example, ignition near the lean flammability limit is one of the challenges for ultra-lean combustion which can greatly improve the thermal efficiency of SIE (Tsuboi et al. 2019). There are different types of ignition (autoignition and forced ignition) in different kinds of reactants (premixed or non-premixed, with and without phase change) under different flow conditions (laminar or turbulent) (Lewis and von Elbe 1961; Mastorakos 2009, 2017). Aiming at assessing the flow effect on flame ignition, this work focuses on forced ignition of a gaseous premixture in a laminar flow.

Most of previous studies on laminar premixed flame ignition considered a quiescent mixture, for which the minimum ignition energy (MIE) was determined by many theoretical, numerical and experimental works (see Chen et al. 2011; Lewis and von Elbe 1961; Ronney 1994; Yu and Chen 2021 and references therein). However, ignition process usually occurs in a flowing mixture. The flow may affect ignition by altering local coupling between molecular/convective heat and mass transport and chemical reactions occurring inside and around the ignition kernel.

Recently, several studies have been conducted on ignition in flowing mixtures (Baum and Poinot 1995; Beduneau et al. 2003; Kobayashi et al. 2019; Bonebrake et al. 2020; Katta et al. 2021; Jo and Gore 2021) simulated ignition in a constant speed flow and found that the minimal ignition power changes nearly linearly with the flow speed. Beduneau et al. (2003) reported MIE data obtained using laser-induced ignition in laminar methane/air mixtures. They found that the MIE increases and decreases with the flow velocity for fuel-rich and fuel-lean cases, respectively. Kobayashi et al. (2019) studied laser-induced spark ignition in dimethyl ether/air mixtures with low velocity. They found that low flow velocity can promote ignition and reduce the MIE since the entrainment of unburnt gas into ignition kernel facilitates the chemical reaction. Katta et al. (2021) simulated the ignition kernel propagation in flowing CH₄/air/diluent mixtures. They highlighted the role of convection on ignition kernel development. In order to quantify the effects of convective flow on MIE, Jo and Gore (2021) analyzed the energy balance at ignition and found that the MIE increases with increasing bulk velocity due to the convective heat loss. These studies indicate that the forced convection brings more unburnt mixtures into the ignition kernel and also increases the heat exchange with the ambient environment. Therefore, the local flow has both positive and negative effects on flame ignition.

These studies (Baum and Poinot 1995; Beduneau et al. 2003; Bonebrake et al. 2020; Jo and Gore 2021; Katta et al. 2021; Kobayashi et al. 2019) only considered uniform flow, whereas ignition usually occurs in flows with strong non-uniformity. Though there are many studies on ignition in turbulent flows (e.g., Mastorakos 2009; Shy et al. 2021), it is very difficult to interpret the effects of turbulence on ignition kernel development. The ignition kernel development is strongly affected by strain rate and its coupling with the differential diffusion of heat and mass (i.e. the Lewis number effect) (Chen et al. 2011; Chakraborty et al. 2008; Turquand d'Auzay et al. 2019; Pouech et al. 2021) emphasized that large unsteady strain rates are crucial for successfully ignition. The canonical configuration of a laminar counterflow provides a well-defined flow field and preserves the similarity with the local flow in turbulent combustion. Besides, the laminar counterflow

allows for neatly quantification of the influence of strain rate on forced ignition, which is very challenging for a turbulent case. To our knowledge, in the literature there is little work on premixed flame ignition in a counterflow. The ignition kernel evolution and MIE in a strained flow are still not well understood.

The above-mentioned considerations motivate the present work, which is to investigate ignition kernel development and MIE in a premixed counterflow. Similar research on forced ignition have been performed experimentally and numerically in a non-premixed counterflow (Ahmed et al. 2007; Richardson and Mastorakos 2007; Wei et al. 2018), in which the variation of mixture fraction plays a major role in the determination of the MIE. The local flow brings the hot gas kernel into mixtures with high reactivities, and possibly triggers successful ignition even through the energy is deposited into unfavorable mixture conditions (Ahmed et al. 2007). The consideration of a premixed counterflow isolates the variation in mixture component and permits us to focus on the interaction between flow field and flame kernel. In the recent work of Yu et al. (2021) and Yu and Maas (2021), the effects of strain rate on MIE of lean methane/air mixtures were examined numerically. They found that the MIE increases with the strain rate. However, their one-dimensional formulation cannot capture the change in flame kernel shape and related flame stretch interaction.

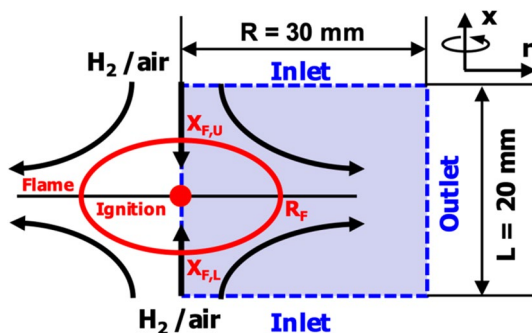
The ignition outcome is determined by the balance between heat generation and heat loss, where the differential diffusion between heat and mass (quantified by the Lewis number, Le) plays an important role (Chen et al. 2011). For large Le , the highly positive stretch of the expanding ignition kernel greatly reduces the flame strength and flame speed, and thereby the transition of an embryonic flame kernel into an expanding flame is very difficult and a large ignition energy is required to achieve successful ignition (Chen et al. 2011). The interaction of local stretch of the expanding ignition kernel and differential diffusion controls critical ignition. Wu et al. (2014) found that turbulence facilitated ignition can be observed at low turbulence intensity due to such interaction. Therefore, two-dimensional simulations need to be conducted to obtain deep understanding of forced ignition in a premixed counterflow. The objectives of this study are to investigate the transient ignition kernel development and to assess the effects of strain rate on the ignition of a premixture with large effective Lewis number, Le .

Usually fuel-lean mixtures of large hydrocarbons are used in engines and they have $Le > 1$. Since the size of detailed chemistry for large hydrocarbons is very large, hydrogen is considered here in order to reduce the computational cost. To achieve large Le , we consider a fuel-rich ($\phi = 5.1$) H_2 /air mixture with $Le \approx 2.3$ (Wu et al. 2014). Here Le is the effective Lewis number of the mixture, and it can be evaluated based on the Markstein length as described in Refs. (Matalon et al. 2003; Law 2006). Note that the chemistry of large hydrocarbons is certainly different from that of hydrogen. However, the development of the highly stretched ignition kernel is mainly affected by the Lewis number rather than the high-temperature chemistry. Therefore, it is expected that the present findings are also qualitatively applicable to fuel-lean mixtures of large hydrocarbons.

2 Numerical Model and Methods

We consider the forced ignition of a H_2 /air mixture in a 2D axisymmetric counterflow as shown in Fig. 1.

Fig. 1 Schematics of flame ignition in a counterflow



The transient ignition process is simulated using the code developed based on OpenFOAM by (Zirwes et al. 2018, 2020). The governing equations for compressible reactive flow are solved using the finite volume method. Cantera (Goodwin et al. 2021) is integrated to evaluate the reaction rates and thermal and transport properties. Detailed hydrogen chemistry developed by Li et al. (2004) is adopted. The mixture-averaged transport model is used for the diffusion velocity. This code was validated in recent studies on premixed flames (Wang et al. 2021; Zirwes et al. 2021a and 2021b). The details on numerical methods and code validation can be found in Refs. (Zirwes et al. 2018, 2020) and thereby are not repeated here.

As shown by the grey region in Fig. 1, the computational domain is $L \times R = 20 \times 30 \text{ cm}^2$. A uniform velocity, U_{in} , is prescribed on the top and bottom inlet boundaries, where the H_2/air mixture ($\varphi = 5.1$) flows into the domain. Symmetric and outlet boundaries are imposed at the left and right sides, respectively. A converged numerical solution for steady, frozen counterflow is first obtained and used as the initial condition. The mixture is initially at $T_u = 298 \text{ K}$ and $P = 1 \text{ atm}$. The global strain rate is $a_g = 4U_{in}/L$ (Seshadri and Williams 1978).

In simulations, the mixture is ignited through energy deposition given by the following source term in the energy equation:

$$q_i = \frac{3E_{ig}}{4\pi r_{ig}^3 \tau_{ig}} \text{ for } t \leq \tau_{ig}, \sqrt{(r - r_{ign})^2 + (x - x_{ign})^2} \leq r_{ig} \quad (1)$$

where $\tau_{ig} = 0.2 \text{ ms}$ is the duration of energy deposition, $r_{ig} = 0.2 \text{ mm}$ the radius of the energy deposited region, and E_{ig} the ignition energy. The center of the ignition kernel is placed at $(r = r_{ign}, x = x_{ign})$. To achieve axis-symmetry, we set $r_{ign} \equiv 0$. We adopt a uniform mesh of $50 \mu\text{m}$. The reaction zone is always covered by more than 15 grid points and grid convergence is ensured. In order to accurately resolve the transient energy deposition and the following thermal runaway processes, a two-level mesh refinement is employed for the initial ignition kernel.

3 Results and Discussion

Ignition processes at different strain rates are simulated. For comparison, we also consider the case with zero strain rate ($a_g = 0$), i.e., ignition in a quiescent mixture. For $a_g > 0$, the counterflow enhances the convective heat and mass transfer inside and around the ignition

kernel and thereby affects the ignition kernel development and MIE. For the expanding flame in a counterflow, there are two characteristic directions: the axial direction along $r=0$ (the upper and lower flame positions are $X_{F,U}$ and $X_{F,L}$, see Fig. 1) and the radial direction along $x=0$ (the flame radius is R_F , see Fig. 1). Along the axial direction, the flame propagates against the inlet unburnt mixture, and it is stabilized as a traditional premixed counterflow flame when the laminar flame speed balances with the local incoming flow. Along the radial direction, the premixed flame propagates in the same direction as the local flow, and thereby the flow accelerates the propagation of the ignition front into the downstream unburnt mixtures.

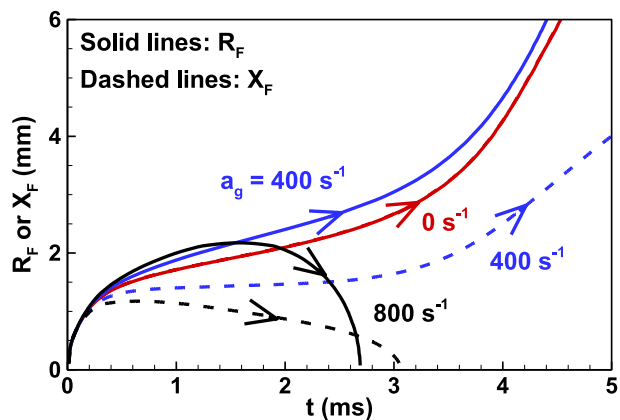
3.1 Effects of Strain rate

We first consider the ignition at the stagnation point, i.e. $r_{ign} = x_{ign} = 0$ mm, where the ignition kernel is subjected to minimal convective heat loss due to the low velocity there. Due to symmetry, we have $X_{F,U} = X_{F,L}$ which is simply denoted as X_F . Three cases with the same ignition energy, $E_{ig} = 0.603$ mJ, but different global strain rates, $a_g = 0, 400$ and 800 s⁻¹, are investigated. To quantify the ignition kernel propagation, we track the flame front positions along the axial and radial directions, X_F and R_F , which are defined based on the local maximum heat release rate. The results are shown in Fig. 2.

A spherically expanding flame is successfully ignited in the quiescent mixture. The flame has the same propagation speed in each direction due to spherical symmetry. The introduction of the counterflow breaks the symmetry. As shown in Fig. 2, for the successful ignition at relatively low strain rate of $a_g = 400$ s⁻¹, the flame in radial (axial) direction propagates faster (slower) than its counterpart in a quiescent mixture. This is due to the different flow directions relative to the flame front in the counterflow, which was mentioned before and indicated in Fig. 1. The larger the strain rate, the stronger the difference between propagation speeds of flames in radial and axial directions. For large strain rate of $a_g = 800$ s⁻¹, the ignition kernel first expands, then shrinks and finally extinguishes, indicating ignition failure. Therefore, higher ignition energy is required for larger strain rate.

To further demonstrate the effects of strain rate on ignition kernel development, Fig. 3 shows the heat release rate distribution at $t = 1.5$ ms. The animation of the heat release rate distribution during the entire ignition process is shown in the Supplementary Material. Figure 3 shows that the counterflow squeezes the ignition kernel from a

Fig. 2 Evolution of ignition kernel in both axial and radial directions for $E_{ig} = 0.603$ mJ and different global strain rates



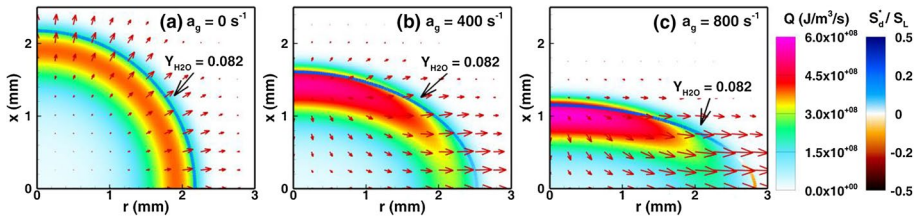


Fig. 3 The heat release rate contours at $t = 1.5$ ms for different global strain rates. The solid lines represent the iso-line of $Y_{\text{H}_2\text{O}} = 0.082$ with their color representing the magnitude of density weighted displacement speed. The red arrows are the energy flux vectors and their lengths are proportional to the magnitude of energy flux. See also the animation in the Supplementary material

sphere to an oblate spheroid. This is because the counterflow inhibits the flame propagation in the axial direction, whereas it promotes the flame propagation along the radial direction, leading to a more flattened ellipsoid at higher strain rate. Compared to the spherically expanding flame, the counterflow exerts opposite effects on flames in the axial and radial directions. For the axial flame, the flame front curvature is greatly reduced by the counterflow, and thereby the flame is strengthened for fuel-rich H_2/air with large Lewis number. In contrast, the radial flame is subjected to very large curvature and thereby is greatly weakened. Consequently, the radial flame has a much lower heat release rate than the axial flame at the same strain rate and the spherically expanding flame at $a = 0 \text{ s}^{-1}$.

The density weighted displacement speed, S_d^* , considers the integrated effects of diffusion and reaction, and can quantify the flame propagation speed relative to local flow (Groot et al. 2002; Giannakopoulos et al. 2015; Böttler et al. 2021). We adopt the iso-surface of H_2O mass fraction in the evaluation of S_d^* :

$$S_d^* = \frac{\rho S_d}{\rho_u} = - \left[\frac{\omega_{\text{H}_2\text{O}}}{\rho_u |\nabla Y_{\text{H}_2\text{O}}|} + \frac{\nabla \cdot (\rho D_{\text{H}_2\text{O}} \nabla Y_{\text{H}_2\text{O}})}{\rho_u |\nabla Y_{\text{H}_2\text{O}}|} \right] \quad (2)$$

where ρ is the density, ρ_u the density of unburnt mixture, $\omega_{\text{H}_2\text{O}}$ the production rate of H_2O , and $D_{\text{H}_2\text{O}}$ the mass diffusivity coefficient of H_2O . The representative iso-surface of $Y_{\text{H}_2\text{O}} = 0.082$ is chosen since its position is close to that of the local maximum heat release rate in the unstretched laminar planar flame. Figure 3 shows that the flame in the axial direction is greatly enhanced and its large positive displacement speed increases with the strain rate. At the initial stage, the ignition kernel is small, and the influence of curvature on local flame speed is dominant compared to the strain rate. The increase of global strain rate significantly reduces the local flame curvature for the axial flames. Therefore, even though the axial flame is subject to a larger positive strain rate at $a_g = 800 \text{ s}^{-1}$, the local displacement speed is larger than that at $a_g = 400 \text{ s}^{-1}$. However, the flame in the radial direction is significantly weakened and its displacement speed is close to zero for $a_g = 400 \text{ s}^{-1}$. Further increase in strain rate to $a_g = 800 \text{ s}^{-1}$ leads to the negative displacement speed as shown in Fig. 3c. The radial flame is pushed by local flow in the radial direction; and it serves as a heat sink and induces ignition failure for $a_g = 800 \text{ s}^{-1}$.

To visualize the energy transport, the energy flux vector proposed by Hooman (2010) is used and it is defined as

$$\vec{E} = \rho c_p \vec{v} (T - T_{\text{ref}}) - k \vec{\nabla} T \quad (3)$$

where c_p is the specific heat capacity at constant pressure, k the thermal conductivity, and $T_{\text{ref}} = 298$ K the reference temperature. Similar to the velocity vector representing streamlines, the energy flux vector shown in Fig. 3 indicates energy transfer streamlines (Hooman 2010). Including both convection and diffusion (see the first and the second term on the right-hand side of Eq. 3), the energy flux vector represents the net energy transfer rate along a specific direction.

For the spherically expanding flame shown in Fig. 3a, the energy flux vector is oriented normal to the flame front and thereby there is no energy transfer between different parts of the flame. However, the situation changes when there is a counterflow. Along the flame front, the angle between convective and diffusive energy flux varies from $-\pi$ to π . There is a stagnation point for energy transfer on the axis of symmetry, where the temperature change is controlled purely by local chemical reaction. The energy flux vectors in Fig. 3b and c clearly show the energy transfer path from the strong axial flame to the weak radial flame. The convective energy transfer increases with the strain rate. At relative high strain rate of $a_g = 800 \text{ s}^{-1}$, the energy is transferred away from the axial flame mainly by convection, which subsequently induces ignition failure. The above results indicate that the counterflow not only changes the local flame curvature but also has great impact on energy transfer.

To investigate the dynamics of the weak radial flame, we conduct the transport budget analysis along the stagnation plane (i.e. $x = 0$) at $t = 1.5$ ms. Figure 4 shows that the influence of convection increases with the strain rate. For $a_g = 0$, the spherical flame propagation is mainly driven by diffusion and reaction. With the increase of strain rate, convection first thickens the preheat zone (see $a_g = 400 \text{ s}^{-1}$) and then participates in the energy balance within the reaction zone (see $a_g = 800 \text{ s}^{-1}$) to support the outwardly propagation of the radial flame through the enhanced preheating of unburnt mixtures downstream. It is

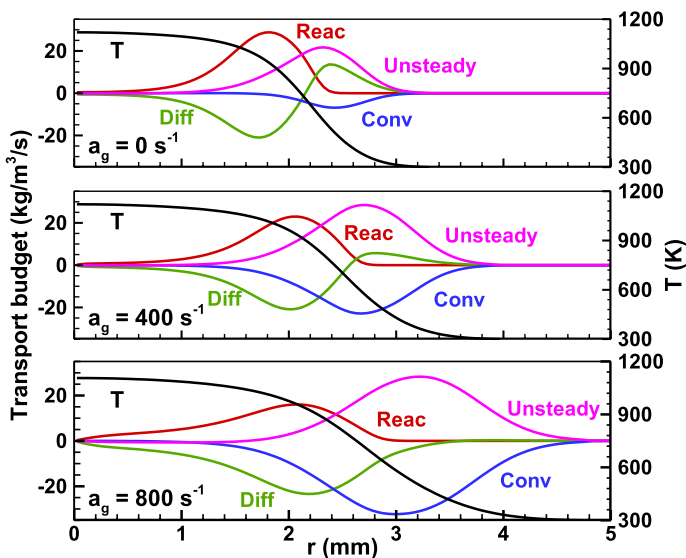
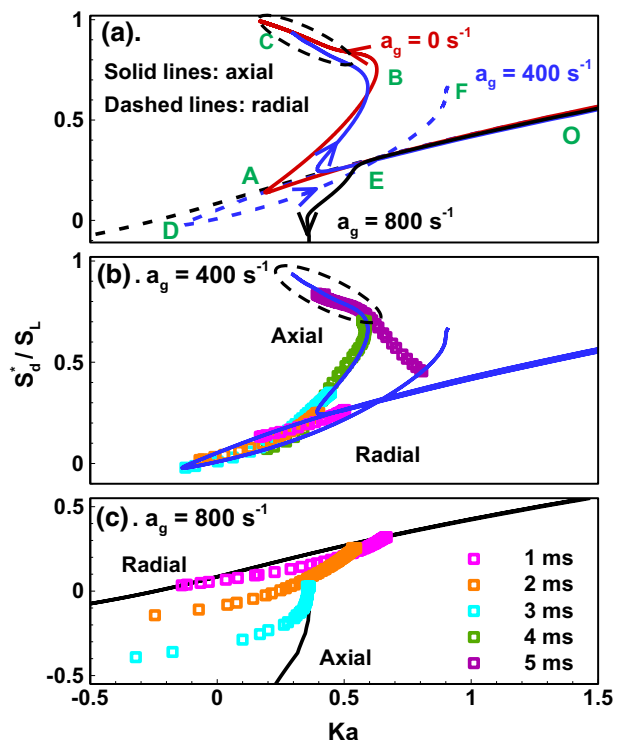


Fig. 4 Profiles of convection, diffusion, reaction and unsteady terms in the energy equation along the stagnation plane (i.e. $x = 0$) at $t = 1.5$ ms for different global strain rates

noted that large local flow velocity reduces the residence time and thereby prevents the flame to propagate in a quasi-steady manner, manifested in the long unsteady transition period for the radial flame (to be shown in Fig. 5). If the energy gain from convection is insufficient to compensate the loss, the radial flame extinguishes. Therefore, to achieve successful ignition at high strain rate, a strong anchored axial flame needs to be formed to resist the energy loss along the radial direction.

Figure 5 shows the change of the normalized displacement speed with the Karlovitz number defined as $Ka = K\delta/S_L$, where K is the local stretch rate, and δ and S_L are respectively the flame thickness and laminar flame speed of the H_2 /air mixture at $\phi = 5.1$. Both S_d^* and Ka are evaluated along the iso-surface of $Y_{H_2O} = 0.082$. Figure 5 only shows the results for flames in the axial and radial direction. For successful ignition at $a_g = 400 \text{ s}^{-1}$, the propagation of the axial flame follows the Z-shaped curve, OABC as marked in Fig. 5a, which is similar to the spherically expanding flame at $a_g = 0$. Such Z-shaped curve was also observed in previous studies for mixtures with large Lewis number (Chen et al. 2021; Wang et al. 2019). The propagation of the radial flame follows the curve OADEF in Fig. 5a, which is totally different from the Z-shaped curve. Near the outmost position along radial direction, the local curvature is much larger than that for the axial flame. Therefore, the flame undergoes a much longer unsteady transition period before becoming self-sustained and entering the quasi-steady regime. Along the radial direction, the premixed flame propagation (S_d) is simultaneously advected by the local flow (u), i.e., $dR_f/dt = S_d + u$, except that S_d is small at large strain rates due to large local curvature. The custom scaling law for premixed flame, i.e. $S_u/S_b = \rho_b/\rho_u$,

Fig. 5 Change of the normalized displacement speed S_d^* with the Karlovitz number Ka . **a** Only shows the results for flames in the axial (i.e., $r=0$) and radial (i.e., $x=0$) directions; and **b** and **c** Shows the results for flames in all directions. The solid lines represent the temporal variation of the axial flame and the radial flame, and the colored symbols represent the spatial variation of the flame at certain times, i.e., $t = 1 \sim 5 \text{ ms}$. The lines and symbols lying in the ellipses represent flames propagating in a quasi-steady manner



rather than that for triple flame speed, i.e., $S_{tri}/S_L = (\rho_b/\rho_u)^{1/2}$ (Ruetsch et al. 1995), is applicable for the this weak flame branch at small strain rates.

The results for flames in all directions and at different times are shown in Fig. 5b and c. At the same time, different parts of the flame may undergo different transition stages. For an example, at $t=4$ ms and $a_g = 400$ s⁻¹, the axial flame enters the quasi-steady propagation region, whereas other parts of the flame still lie in the unsteady transition region. It is clear that the linear dependence of displacement speed on stretch rate at low Karlovitz number (Matalon and Matkowsky 1982) is still applicable, indicating that the acceleration mechanism of triple flame is absent considering the homogeneous mixture in the present configuration (Ruetsch et al. 1995; Chung 2007). Besides, Fig. 5c shows that negative flame stretch and negative displacement speed appear due to the local flame extinction. Therefore, forced ignition in strained flows can pose challenges to flamelet modeling.

For all the results above, the ignition energy is fixed to be $E_{ig} = 0.603$ mJ. The MIE at different strain rates is determined by the trial-and-error method and the relative error is within 5%. The results are shown in Fig. 6. The flame temperature, T_{max} , for the corresponding premixed counterflow flame is also plotted, which indicates the extinction strain rate, $a_{ex} = 1689$ s⁻¹. The MIE is shown to increase monotonically with the strain rate. At low strain rate with $a_g \leq 400$ s⁻¹, the MIE remains nearly constant with the relative increase below 5%. When the strain rate is close to the extinction value, the MIE rises rapidly. To illustrate the differential diffusion (Lewis number) on premixed flame ignition in a counterflow, we calculate the MIE for the same H₂/air mixture but with unity Lewis number diffusion, which is achieved by manually setting the diffusion coefficients of all species equal to the thermal diffusivity, i.e., $D_{k,m} = D_T = \lambda/\rho c_p$. Figure 6 shows that for $Le = 1$, the MIE is significantly reduced and is nearly constant. Note that for $Le = 1$, the extinction strain rate a_{ex} increases greatly and the MIE also increases when the strain rate is close to the extinction value. The above results indicate that similar to ignition in a quiescent mixture, the MIE for ignition in a counterflow also strongly depends on Lewis number. Moreover, Fig. 6 also indicates that the effects of Lewis number on ignition in a counterflow become stronger at higher strain rate.

Fig. 6 Change of the MIE and maximum temperature with the strain rate for two ignition positions of $x_{ign} = 0$ and 5 mm

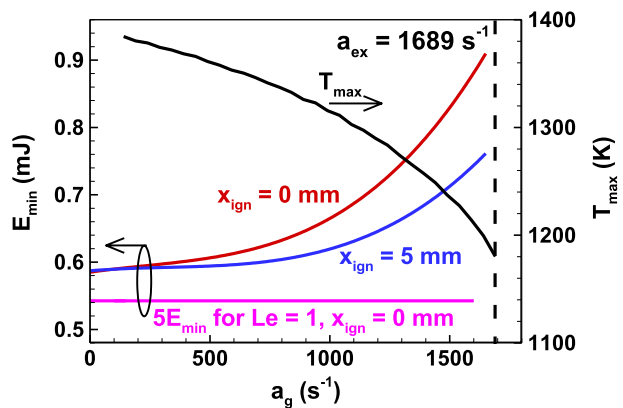


Fig. 7 Evolution of positions of upper and lower axial flames and their distance for same $a_g = 800 \text{ s}^{-1}$ and $E_{ign} = 0.603 \text{ mJ}$ but different ignition positions $x_{ign} = 0$ and 5 mm

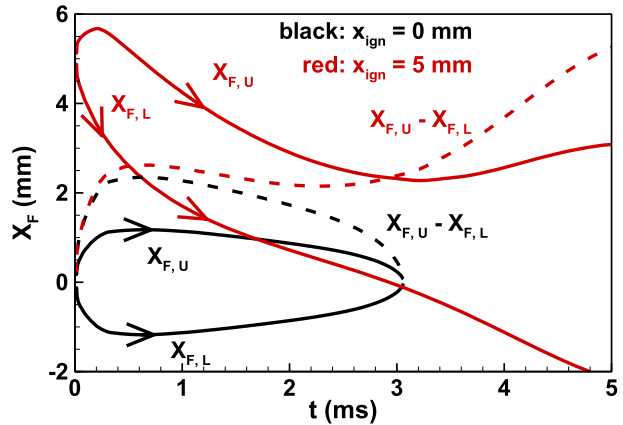
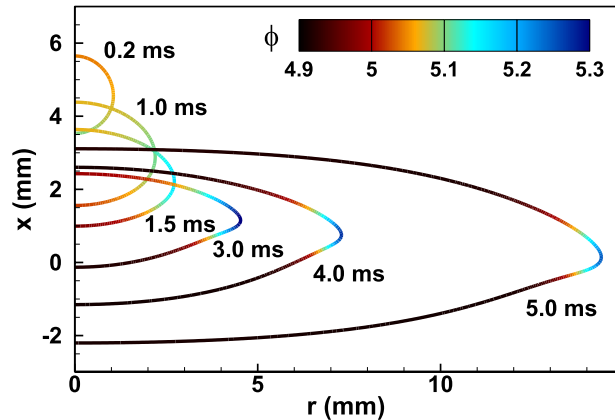


Fig. 8 Evolution of flame front (represented by the iso-line of $Y_{H_2O} = 0.082$) at different times for $a_g = 800 \text{ s}^{-1}$, $E_{ign} = 0.603 \text{ mJ}$ and $x_{ign} = 5 \text{ mm}$. The color represents the local equivalence ratio, which is calculated based on the local elemental mole fractions of H and O and is defined as $\phi = X_H/X_O/(X_H/X_O)_{st} = X_H/2X_O$



3.2 Effects of Ignition Position

The above results are obtained for ignition at the stagnation point, i.e., $x_{ign} = r_{ign} = 0 \text{ mm}$. Around the stagnation point, the flow speed is small which corresponds to a relatively long residence time and low convective transport of heat and mass. Therefore, it could be expected that the stagnation point is the optimum ignition position. Counterintuitively, this is not true. As shown in the following, moving the ignition position away from the stagnation point can promote ignition.

We first consider the same strain rate, $a_g = 800 \text{ s}^{-1}$, and the same ignition energy, $E_{ign} = 0.603 \text{ mJ}$, as before. The previous subsection (see Fig. 2) shows that ignition fails when the ignition kernel is initially at the stagnation point. In contrast, successful ignition is achieved when the ignition position moves upwardly to $x_{ign} = 5 \text{ mm}$. This is demonstrated by the animation of heat release rate distribution in the Supplementary Material B and by Fig. 7.

Figure 7 shows the evolution of the axial flame positions for both the upper and lower branches, i.e., $X_{F,U}$ and $X_{F,L}$, and the distance between them, $X_{F,U} - X_{F,L}$. For $t < 0.3 \text{ ms}$, two dashed lines in Fig. 7 overlap, indicating the ignition position has little influence on the formation of the initial ignition kernel. This is also demonstrated by Fig. 8 which shows

that the ignition kernel is nearly spherical at $t=0.2$ ms. The ignition kernel is then pushed toward the stagnation plane, companioned with the thermal expansion of burnt products. Finally, the upper and lower flames approach to their stabilized states and traditional twin premixed counterflow flames are observed.

Moving the ignition kernel upwards (i.e., $x_{ign} = 5$ mm) breaks the symmetry across the plane at $x=0$ and creates windward (upper) and leeward (lower) flames at the same time. Compared to the upper flame front, the lower flame has a longer residence time and relatively lower local equivalence ratio (see Fig. 8), and thereby it is easier to develop into a self-sustained flame. For the lower branch, the local strain rate is lower and so is the flame-stretch interaction. This is demonstrated by Fig. 9 which shows that the lower flame has much stronger heat release rate than the upper flame. Furthermore, the local equivalence ratio of radial flame is always the largest due to the coupling between positive stretch and large Lewis number. Therefore, Fig. 9 shows that the flame tip propagating in the radial direction has very low heat lease rate and negative displacement speed. Note that the local equivalence ratio is also influenced by the preferential diffusion. The shift in turn influences the reactants' consumption and radicals' production, leading to a change in local flame structure and flame speed.

The influences exerted by the local flow are primarily manifested after the energy deposition and roughly categorized in two aspects, which are demonstrated by the flame front evolution shown in Fig. 8. One is the overall downward shift of the ignition kernel, and the other is the compression of the ignition kernel, leading to flattening. It is noted that the former is absent for ignition at the stagnation point. The ignition kernel is squeezed by the inlet flow from both sides, leading to a more flattened ellipsoid. The compression effect can be effectively reduced by the downward movement of the ignition kernel, which happens only for ignition away from the stagnation point. Shown in Figs. 8 and 9a, the ignition kernel at $t=1.5$ ms is mainly subjected to compression from the upper side while there is little contribution from the lower inlet stream. As the ignition kernel moves downward, Figs. 8 and 9b show that at $t=3$ ms the contribution from the lower sider is no longer negligible. The distance between the upper and lower flames, $X_{F,U} - X_{F,L}$, quantifies the flatness of the ignition kernel. Compared to ignition at the stagnation point (i.e., $x_{ign} = 0$ mm), ignition at $x_{ign} = 5$ mm corresponds to a larger distance (see dashed lines in Fig. 7) and thereby

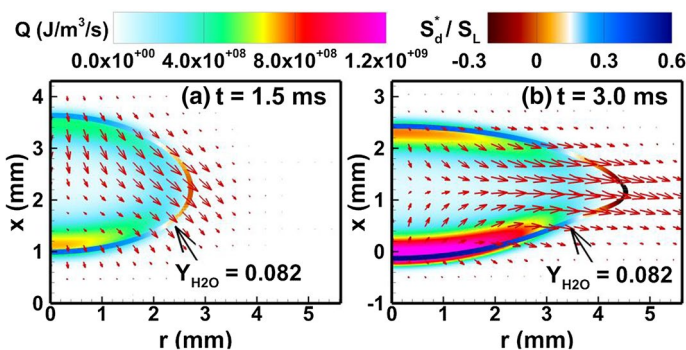


Fig. 9 The heat release rate contours at **a** $t=1.5$ ms and **b** $t=3.0$ ms for $a_g = 800 \text{ s}^{-1}$, $E_{ign}=0.603 \text{ mJ}$ and $x_{ign} = 5$ mm. The solid lines represent the iso-line of $Y_{H_2O} = 0.082$ with their color representing the magnitude of normalized, density weighted displacement speed. The red arrows are the energy flux vectors and their lengths are proportional to the magnitude of energy flux. See also the animation in the Supplementary material

a less flat flame shape, which reduces the curvature of the flame tip propagating in the radial direction and thereby strengthens this flame tip. Consequently, successful ignition is achieved for $x_{ign} = 5$ mm. Its transition to obtain a steady counterflow flame takes about 6 ms.

To further interpret the effects of ignition position, the density weighted displacement speed, curvature and strain rate data are uniformly sampled along the flame surface (i.e., the iso-line of $Y_{H_2O} = 0.082$), and the probability density distribution is computed based on the spatial distribution of the 2D flame at $t = 1.5$ ms (the iso-line of $Y_{H_2O} = 0.082$ in Fig. 9a). The results are displayed in Fig. 10. There are three local peaks for displacement speed for $x_{ign} = 5$ mm. The middle and rightmost peaks respectively correspond to the upper and lower axial flames, both of which have small curvature and thereby is mainly affected by hydrodynamic strain rate. Compared to the upper axial flame, the lower axial flame is exposed to weaker hydrodynamic strain (see Figs. 9a and 10c) and has larger displacement speed. The leftmost peak in Fig. 10a corresponds to the weakest flame with the largest curvature, which is the flame tip propagating in the radial direction. Note that at this outmost position the local strain rate is almost negligible while the curvature is large. Figure 10b shows that the curvature range is greatly reduced by moving the ignition position from $x_{ign} = 0$ mm to $x_{ign} = 5$ mm. This is consistent with the statements made in the previous paragraph.

Similar to Fig. 5a, Fig. 11 plots the results for $x_{ign} = 5$ mm. The Z-shaped curve is obtained for both the upper and lower axial flames. Compared to the results for $a_g = 400$ s⁻¹ shown in Fig. 5b, the data in Fig. 11 are more broadly distributed. The imposed

Fig. 10 Distribution of **a** normalized density weighted displacement speed, **b** non-dimensional curvature and **c** Karlovitz number defined with strain rate, i.e., $Ka_s = (-nn : \nabla v + \nabla \cdot n)\delta_f/S_L$, along the flame front (defined as iso-line of $Y_{H_2O} = 0.082$) at $t = 1.5$ ms for $a_g = 800$ s⁻¹, $E_{ig} = 0.603$ mJ

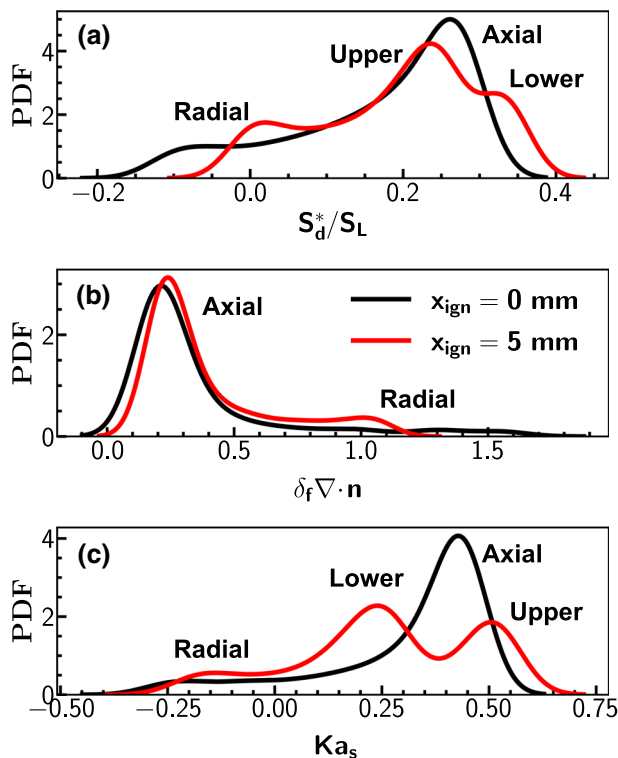
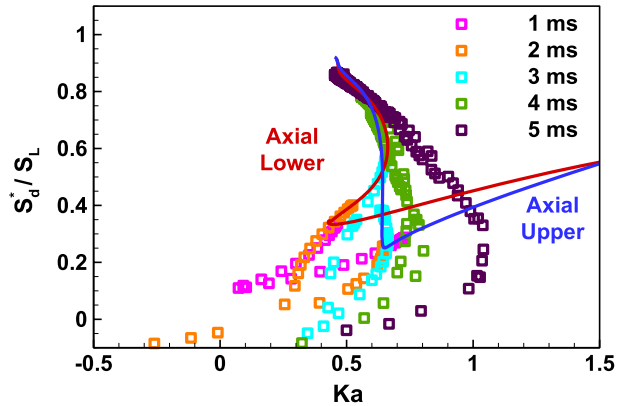


Fig. 11 Change of normalized displacement speed S_d^* with the Karlovitz number Ka for flames in all directions and at different times. $a_g = 800 \text{ s}^{-1}$, $E_{ign} = 0.603 \text{ mJ}$ and $x_{ign} = 5 \text{ mm}$. The solid lines represent the results for the upper (blue) and lower (red) axial flames, and the colored symbols represent the spatial variation of flame at certain times, i.e., $t = 1 \sim 5 \text{ ms}$



global strain rate influences the termination point of the Z-shaped curvature for the axial flames, since this point represents the final stabilized diffusion flame state. Furthermore, Fig. 11 shows that successful ignition does not guarantee positive displacement speed everywhere. As mentioned before, the flame tip propagating in the radial direction has a very large curvature and thereby it has a negative displacement speed since $Le > 1$.

We also calculate the MIE for different strain rates but fixed ignition position of $x_{ign} = 5 \text{ mm}$. The results are plotted in Fig. 6, which shows that moving the ignition position away from the stagnation point can reduce the MIE and thereby promote ignition. For $a_g < 400 \text{ s}^{-1}$, the strain rate has little influence on the MIE and so does the movement of the ignition position. For $a_g > 400 \text{ s}^{-1}$, the reduction in MIE caused by moving the ignition position from $x_{ign} = 0 \text{ mm}$ to $x_{ign} = 5 \text{ mm}$ is clearly observed and it increases with the strain rate. This is because at higher strain rate, the compression of the ignition kernel is stronger and the flame tip propagating in the radial direction has a larger curvature. Moving the ignition position away from the stagnation point can induce larger reduction in the curvature at higher strain rate. Note that the presence of the counterflow increases the MIE mainly due to the extinction of the highly curved radial flame. The ignition enhancement via moving the ignition position away from the stagnation point is mainly caused by the reduction of the flame curvature of the radial flame.

4 Conclusion

Two-dimensional simulations considering detailed chemistry and transport are conducted for forced ignition of a fuel-rich H_2/air mixture ($\varphi = 5.1$, $Le \approx 2.3$) in a laminar counterflow. The transient ignition kernel development and the MIE at different strain rates and different ignition positions are investigated.

The counterflow is shown to have great impact on ignition kernel development and MIE for mixtures with large Le . The counterflow compresses the ignition kernel and changes its shape from a sphere to an oblate spheroid. Compared to the spherically expanding flame in a quiescent mixture, the curvature of the upper and lower axial flames is greatly reduced by the counterflow, and thereby for fuel-rich H_2/air with $Le > 2$ the axial flame is strengthened. On the contrary, the radial flame is subjected to very large curvature induced by the counterflow, and thereby is greatly weakened. Besides, the counterflow also has great impact

on energy transfer. The energy flux vector shows that the weak radial flame relies on the convective energy transfer from the axial flame. With the increase of strain rate, the radial flame has negative displacement speed and extinguishes. Therefore, for $Le > 2$, the ignition becomes more difficult at higher strain rate. To achieve successful ignition in mixtures with large Le and at high strain rate, a strong anchored axial flame needs to be formed to resist the energy loss along the radial direction.

Counterintuitively, it is found that moving the ignition position away from the stagnation point can reduce the MIE and thereby promote ignition for the present mixture with large Le . Moving the ignition position above the stagnation point can efficiently reduce the curvature of the flame tip propagating in the radial direction and thereby strengthens this flame tip. Besides, moving the ignition position upwards also strengthens the lower axis flame via increasing the local residence time, decreasing the convective heat transfer and moving the local equivalence ratio toward stoichiometric case. For relatively low strain rate, both strain rate and ignition position have little influence on the MIE. At relatively high strain rate, the MIE is reduced after changing ignition position from $x_{ign} = 0$ mm to $x_{ign} = 5$ mm and the reduction increases with the strain rate.

The change of the density-weighted displacement speed with the Karlovitz number is studied for the transient ignition process. A Z-shaped curve is obtained as in previous studies for large Le . The unsteadiness is clearly shown and negative displacement speed is observed, which can pose challenges to flamelet modeling of forced ignition under strained conditions and deserves further study.

This work is a first step towards a better understanding ignition of mixtures with $Le > 2$ in strained flows. In future works, it would be interesting to consider more complicated flows and turbulence.

Supplementary Information The online version contains supplementary material available at <https://doi.org/10.1007/s10494-022-00374-2>.

Acknowledgements This research was funded by NSFC, China (Nos. 51861135309, 52176096) and DFG, German (No. 411275182). We thank Drs. Thorsten Zirwes, Feichi Zhang, and Henning Bockhorn at Karlsruhe Institute of Technology for providing us their EBI-DNS code.

Author Contributions SX and ZC conceived and planned the simulations. SX conducted simulations and analysis, prepared the figures and wrote the original draft. XY, HB and AS analyzed the data. CH and ZC supervised the project. All authors discussed the results and reviewed the manuscript.

Funding This research was funded by NSFC, China (Nos. 51861135309, 52176096) and DFG, German (No. 411275182). The authors have no relevant financial or non-financial interests to disclose.

Declarations

Conflict of interest The authors declare that they have no known competing financial interests or personal relationships that could have appeared to influence the work reported in this paper.

References

- Ahmed, S.F., Balachandran, R., Mastorakos, E.: Measurements of ignition probability in turbulent non-premixed counterflow flames. *Proc. Combust. Inst.* **31**, 1507–1513 (2007). <https://doi.org/10.1016/j.proci.2006.07.089>
- Baum, M., Poinso, T.: Effects of mean flow on premixed flame ignition. *Combust. Sci. Technol.* **106**, 19–39 (1995). <https://doi.org/10.1080/00102209508907765>

- Beduneau, J.-L., Kim, B., Zimmer, L., Ikeda, Y.: Measurements of minimum ignition energy in premixed laminar methane/air flow by using laser induced spark. *Combust. Flame* **132**, 653–665 (2003). [https://doi.org/10.1016/S0010-2180\(02\)00536-9](https://doi.org/10.1016/S0010-2180(02)00536-9)
- Bonebrake, J.M., Ombrello, T.M., Blunck, D.L.: Effect of CO₂ dilution on forced ignition and development of CH₄/air ignition kernels. *Combust. Flame* **222**, 242–251 (2020). <https://doi.org/10.1016/j.combustflame.2020.08.046>
- Böttler, H., Scholtissek, A., Chen, X., Chen, Z., Hasse, C.: Premixed flames for arbitrary combinations of strain and curvature. *Proc. Combust. Inst.* **38**, 2031–2039 (2021). <https://doi.org/10.1016/j.proci.2020.06.312>
- Chakraborty, N., Hawkes, E., Chen, J., Cant, R.: The effects of strain rate and curvature on surface density function transport in turbulent premixed methane–air and hydrogen–air flames: a comparative study. *Combust. Flame* **154**, 259–280 (2008). <https://doi.org/10.1016/j.combustflame.2008.03.015>
- Chen, X., Böttler, H., Scholtissek, A., Hasse, C., Chen, Z.: Effects of stretch-chemistry interaction on chemical pathways for strained and curved hydrogen/air premixed flames. *Combust. Flame* **232**, 111532 (2021). <https://doi.org/10.1016/j.combustflame.2021.111532>
- Chen, Z., Burke, M.P., Ju, Y.: On the critical flame radius and minimum ignition energy for spherical flame initiation. *Proc. Combust. Inst.* **33**, 1219–1226 (2011). <https://doi.org/10.1016/j.proci.2010.05.005>
- Chung, S.H.: Stabilization, propagation and instability of tribrachial triple flames. *Proc. Combust. Inst.* **31**, 877–892 (2007). <https://doi.org/10.1016/j.proci.2006.08.117>
- Giannakopoulos, G.K., Gatzoulis, A., Frouzakis, C.E., Matalon, M., Tomboulides, A.G.: Consistent definitions of “flame displacement speed” and “Markstein length” for premixed flame propagation. *Combust. Flame* **162**, 1249–1264 (2015). <https://doi.org/10.1016/j.combustflame.2014.10.015>
- Goodwin, D.G., Speth, R.L., Moffat, H.K., Weber, B.W.: Cantera: An object-oriented software toolkit for chemical kinetics, thermodynamics, and transport processes, (2021). <https://zenodo.org/record/4527812>
- Groot, G.R.A., van Oijen, J.A., de Goey, L.P.H., Seshadri, K., Peters, N.: The effects of strain and curvature on the mass burning rate of premixed laminar flames. *Combust. Theory Model.* **6**, 675–695 (2002). <https://doi.org/10.1088/1364-7830/6/4/307>
- Hooman, K.: Energy flux vectors as a new tool for convection visualization. *Int. J. Numer. Methods Heat Fluid Flow* **20**, 240–249 (2010). <https://doi.org/10.1108/09615531011016984>
- Jo, S., Gore, J.P.: Laser induced spark ignition of laminar premixed methane air jets. In: AIAA propulsion and energy 2021 forum. American Institute of Aeronautics and Astronautics, VIRTUAL EVENT, Reston (2021)
- Katta, V.R., Bonebrake, J.M., Blunck, D.L., Ombrello, T.M.: Propagation of ignition kernel in CO₂-diluted, CH₄/air mixtures. *Combust. Flame* **229**, 111380 (2021). <https://doi.org/10.1016/j.combustflame.2021.02.026>
- Kobayashi, Y., Nakaya, S., Tsue, M.: Laser-induced spark ignition for DME–air mixtures with low velocity. *Proc. Combust. Inst.* **37**, 4127–4135 (2019). <https://doi.org/10.1016/j.proci.2018.05.011>
- Law, C.K.: Combustion physics. Cambridge University Press, Cambridge; New York (2006)
- Lewis, B., von Elbe, G.: Combustion, flames and explosions of gases. Elsevier, Amsterdam (1961)
- Li, J., Zhao, Z., Kazakov, A., Dryer, F.L.: An updated comprehensive kinetic model of hydrogen combustion. *Int. J. Chem. Kinet* **36**, 566–575 (2004). <https://doi.org/10.1002/kin.20026>
- Mastorakos, E.: Ignition of turbulent non-premixed flames. *Prog. Energy Combust. Sci.* **35**, 57–97 (2009). <https://doi.org/10.1016/j.peccs.2008.07.002>
- Mastorakos, E.: Forced ignition of turbulent spray flames. *Proc. Combust. Inst.* **36**, 2367–2383 (2017). <https://doi.org/10.1016/j.proci.2016.08.044>
- Matalon, M., Cui, C., Bechtold, J.K.: Hydrodynamic theory of premixed flames: effects of stoichiometry, variable transport coefficients and arbitrary reaction orders. *J. Fluid Mech.* **487**, 179–210 (2003). <https://doi.org/10.1017/S0022112003004683>
- Matalon, M., Matkowsky, B.J.: Flames as gasdynamic discontinuities. *J. Fluid Mech.* **124**, 239 (1982). <https://doi.org/10.1017/S0022112082002481>
- Pouech, P., Duchaine, F., Poinot, T.: Premixed flame ignition in high-speed flows over a backward facing step. *Combust. Flame* **229**, 111398 (2021). <https://doi.org/10.1016/j.combustflame.2021.111398>
- Richardson, E.S., Mastorakos, E.: Numerical investigation of forced ignition in laminar counterflow non-premixed methane-air flames. *Combust. Sci. Technol.* **179**, 21–37 (2007). <https://doi.org/10.1080/00102200600805892>
- Ronney, P.D.: Laser versus conventional ignition of flames. *Opt. Eng.* **33**, 510 (1994). <https://doi.org/10.1117/12.152237>
- Ruetsch, G.R., Vervisch, L., Liñán, A.: Effects of heat release on triple flames. *Phys. Fluids* **7**, 1447–1454 (1995). <https://doi.org/10.1063/1.868531>

- Seshadri, K., Williams, F.A.: Laminar flow between parallel plates with injection of a reactant at high Reynolds number. *Int. J. Heat. Mass. Transf.* **21**, 251–253 (1978). [https://doi.org/10.1016/0017-9310\(78\)90230-2](https://doi.org/10.1016/0017-9310(78)90230-2)
- Shy, S., Liao, Y.-C., Chen, Y.-R., Huang, S.-Y.: Two ignition transition modes at small and large distances between electrodes of a lean primary reference automobile fuel/air mixture at 373 K with Lewis number > 1 . *Combust. Flame* **225**, 340–348 (2021). <https://doi.org/10.1016/j.combustflame.2020.11.012>
- Tsuboi, S., Miyokawa, S., Matsuda, M., Yokomori, T., Iida, N.: Influence of spark discharge characteristics on ignition and combustion process and the lean operation limit in a spark ignition engine. *Appl. Energy* **250**, 617–632 (2019). <https://doi.org/10.1016/j.apenergy.2019.05.036>
- Turquand d'Auzay, C., Papapostolou, V., Ahmed, S.F., Chakraborty, N.: On the minimum ignition energy and its transition in the localised forced ignition of turbulent homogeneous mixtures. *Combust. Flame* **201**, 104–117 (2019). <https://doi.org/10.1016/j.combustflame.2018.12.015>
- Wang, Y., Han, W., Chen, Z.: Effects of fuel stratification on ignition kernel development and minimum ignition energy of n-decane/air mixtures. *Proc. Combust. Inst.* **37**, 1623–1630 (2019). <https://doi.org/10.1016/j.proci.2018.05.087>
- Wang, Y., Zhang, H., Zirwes, T., Zhang, F., Bockhorn, H., Chen, Z.: Ignition of dimethyl ether/air mixtures by hot particles: Impact of low temperature chemical reactions. *Proc. Combust. Inst.* **38**, 2459–2466 (2021). <https://doi.org/10.1016/j.proci.2020.06.254>
- Wei, Y., Segura, F.S., Deng, W., Chen, R.-H.: Effect of transport processes on ignition of stretched diffusion flames using laser spark. *Int. J. Heat. Mass. Transf.* **123**, 988–993 (2018). <https://doi.org/10.1016/j.ijheatmasstransfer.2018.03.025>
- Wu, F., Saha, A., Chaudhuri, S., Law, C.K.: Facilitated ignition in turbulence through differential diffusion. *Phys. Rev. Lett.* **113**, 024503 (2014). <https://doi.org/10.1103/PhysRevLett.113.024503>
- Yu, C., Maas, U.: Reaction-diffusion manifolds (REDIM) method for ignition by hot gas and spark ignition processes in counterflow flame configurations. *Combust. Sci. Technol.* (2021). <https://doi.org/10.1080/00102202.2021.2019243>
- Yu, C., Markus, D., Schießl, R., Maas, U.: Numerical study on spark ignition of laminar lean premixed methane-air flames in counterflow configuration. *Combust. Sci. Technol.* (2021). <https://doi.org/10.1080/00102202.2021.2008919>
- Yu, D., Chen, Z.: Theoretical analysis on the transient ignition of a premixed expanding flame in a quiescent mixture. *J. Fluid Mech.* **924**, A22 (2021). <https://doi.org/10.1017/jfm.2021.633>
- Zirwes, T., Zhang, F., Denev, J.A., Habisreuther, P., Bockhorn, H.: Automated code generation for maximizing performance of detailed chemistry calculations in OpenFOAM. In: Nagel, W.E., Kröner, D.H., Resch, M.M. (eds.) *High performance computing in science and engineering*, vol. 17, pp. 189–204. Springer International Publishing, Cham (2018)
- Zirwes, T., Zhang, F., Habisreuther, P., Hansinger, M., Bockhorn, H., Pfitzner, M., Trimis, D.: Quasi-DNS dataset of a piloted flame with inhomogeneous inlet conditions. *Flow. Turbul. Combust.* **104**, 997–1027 (2020). <https://doi.org/10.1007/s10494-019-00081-5>
- Zirwes, T., Häber, T., Zhang, F., Kosaka, H., Dreizler, A., Steinhäuser, M., Hasse, C., Stagni, A., Trimis, D., Suntz, R., Bockhorn, H.: Numerical study of quenching distances for side-wall quenching using detailed diffusion and chemistry. *Flow Turbul. Combust.* **106**, 649–679 (2021a). <https://doi.org/10.1007/s10494-020-00215-0>
- Zirwes, T., Zhang, F., Habisreuther, P., Hansinger, M., Bockhorn, H., Pfitzner, M., Trimis, D.: Identification of flame regimes in partially premixed combustion from a quasi-DNS dataset. *Flow. Turbul. Combust.* **106**, 373–404 (2021b). <https://doi.org/10.1007/s10494-020-00228-9>

Publisher's Note Springer Nature remains neutral with regard to jurisdictional claims in published maps and institutional affiliations.

Springer Nature or its licensor holds exclusive rights to this article under a publishing agreement with the author(s) or other rightsholder(s); author self-archiving of the accepted manuscript version of this article is solely governed by the terms of such publishing agreement and applicable law.